

Generic Predictions for Primordial Perturbations and their implications

Mohit K. Sharma,^{1,*} M. Sami,^{1,2,3,†} and David F. Mota^{4,‡}

¹Centre For Cosmology and Science Popularization (CCSP),
SGT University, Gurugram, Haryana- 122505, India

²Eurasian International Centre for Theoretical Physics, Astana, Kazakhstan

³Chinese Academy of Sciences, 52 Sanlihe Rd, Xicheng District, Beijing

⁴Institute of Theoretical Astrophysics, University of Oslo, P.O. Box 1029 Blindern, N-0315 Oslo, Norway

We introduce a novel framework for studying small-scale primordial perturbations and their cosmological implications. The framework uses a deep reinforcement learning to generate scalar power spectrum profiles that are consistent with current observational constraints. The framework is shown to predict the abundance of primordial black holes and the production of secondary induced gravitational waves. We demonstrate that the set up under consideration is capable of generating predictions that are beyond the traditional model-based approaches.

I. INTRODUCTION

In exploring the origins of gravitational waves and the abundance of primordial black holes within the standard inflationary paradigm, a pivotal question arises: *How can we best realize these phenomena in a model-independent manner, and could artificial intelligence (AI) contribute to this pursuit?* Since the inflationary paradigm have been successful in explaining the origin of density perturbations, flatness of the universe, and the horizon size, it also holds the possibility of anticipating the production of gravitational waves (GWs) and the dense objects like primordial black holes (PBH) [1–8]. However, the usual way to achieve this involves a lot of careful adjustment in the parameter space, and the need for reverse cosmological modeling to match some of the observational evidence often makes the whole picture quite rigid and less general. In order to alleviate these tight restrictions and explore other possibilities within a given framework, we opt for AI based technique.

It may be noted that the AI algorithms have been successful in diverse problem-solving scenarios, their application presents a viable approach to achieve optimal or near-optimal outcomes for the aforementioned inflationary challenges. In order to obtain the outcomes for the standard inflationary scenario, which contains several theoretical constraints, we opt to develop a model-independent framework capable of accommodating and addressing necessary requirements, such as Cosmic Microwave Background (CMB) constraints [9, 10]. One effective approach to constructing a framework is leveraging the benefits of the dimensionless nature of slow-roll parameters. These parameters not only offer insights into the evolution of the background spacetime but also play a crucial role in determining the amplitude of primordial density fluctuations [11–15].

The framework comprises a large $m \times n$ grid structure,

representing the entire range of magnitudes the first slow-roll parameter can assume. Each transition from one cell to another is treated as a transition in time, effectively determining the second slow-roll parameter at a specific time instance. Being unconstrained from any sort of pre-requirements, the framework is capable to make predictions while satisfying the observational constraints. In order to make the predictions, we use the state-of-the-art reinforcement algorithm: Proximal Policy Optimization (PPO) of OpenAI [16]. The main reason to choose this algorithm is its proven track record of being successful in tackling complex problems and its smooth training process. After constructing the framework and completing the training process, the model’s predictions can be evaluated to determine if they exhibit any enhancement in the scalar power spectrum and satisfy the inflationary requirements.

In this paper, our primary goal is not only to examine the predictions of the trained model but also to assess if, at the observational level, it reveals evidence that may not be feasible within conventional cosmological models. Given that the trained model generates predictions without imposing constraints on its predictive nature, it is likely to produce results that are more natural. This is due to the fact that in the standard setup, inflationary scalar field potential parameters are needed to be chosen very precisely, often to three or four decimal places, to create large fluctuations during inflation [17, 18]. Additionally, in models designed to produce multiple enhancements in the primordial power spectrum, selecting parameter values becomes even more difficult. One consequence of this reliance on finely-tuned parameters is that models predicting PBHs for a specific mass scale may not account for the possibility of PBHs with other masses. Therefore, to enhance the predictability of PBH production across different mass ranges and without the need of fine-tuning, we adopt a deep reinforcement learning framework. Given its flexible nature, this approach not only enables the prediction of the abundance of primordial black holes (PBHs) and gravitational waves (GWs) generated from the scalar perturbations but also allows to examine their distribution.

* mrmohit254@gmail.com

† samijamia@gmail.com

‡ d.f.mota@astro.uio.no

The paper is organized as follows: (i) We provide a brief explanation of the working principles of reinforcement learning, (ii) We present a detailed discussion on cosmological inflation within a general framework, and discussing the conditions for large density fluctuations, (iii) We give a detailed explanation of our framework, including the pertinent equations employed to analyze various phenomena, (iv) We examine the predictive results derived from our trained model, and (v) We conclude with final remarks.

II. AN OVERVIEW TO RL

The field of learning techniques is primarily categorized into three main types: (i) supervised, (ii) unsupervised, and (iii) reinforcement learning (RL). While supervised and unsupervised learning involve mapping input data to output categories and utilizing input data alone, respectively, RL distinguishes itself through its unique learning mechanism. RL employs a reward-based technique, interacting with the environment and evaluating the quality of state-action pairs sequentially. Renowned for its effectiveness in handling highly complex nonlinear systems, RL serves as a cornerstone in artificial intelligence. The core principle of RL entails a computer agent interacting with the environment, taking actions, and receiving feedback. Based on the outcomes of these actions, the agent receives rewards or penalties, aiding in the identification of favorable actions at each step. The agent’s ultimate objective is to maximize the accumulated rewards over time.

In a general setup, the agent is guided by an AI algorithm, which, at a specific time step t , observes a state s_t . Executing an action a_t results in a transition to state s_{t+1} . At each time step, the agent receives a reward r_t as feedback. The primary aim of the agent is to acquire knowledge of a policy π (also denoted as a strategy), facilitating the accumulation of the highest possible reward during its exploration in the environment. In each iteration of interaction with the environment, the agent updates its policy based on the preceding rewards, utilizing this information to discern the optimal approach for maximizing overall rewards.

A. Markov Decision Process

The decision on how does the agent will learn in an environment is described by a stochastic process known as the markov decision process (MDP) which consist of the following elements:

- Set of states S and actions A of the environment.
- Transition probability: $T(s_{t+1}|s_t, a_t)$ which maps the state and action at timestep t with the distribution of states at the next time step $t + 1$.

- Reward function $R(s_t, a_t, s_{t+1})$ based on the current action a_t .
- Discount factor: $\gamma \in [0, 1]$ which signifies the weightage to be given to the immediate reward.

The policy π defines a mapping from states to the probability distribution of actions, expressed as $\pi = Pr(a_t|s_t)$. Following each episode, characterized by the completion of a specific number of timesteps, the policy undergoes an update, and the accumulated reward is computed as $R = \sum_{t=1}^T \gamma^t r_t$. The primary objective of this stochastic process is to identify an optimal policy, denoted as π^* , determined as:

$$\pi^* = \underset{\pi}{argmax} (E[R(\pi)]) \quad (1)$$

which aims to maximize the expected reward for the agent.

B. Policy Gradient Technique

There are two ways through which an agent can learn: (i) by learning from the stored past experiences which is known as the offline policy, (ii) by directly learning from whatever the agent encounters in the environment. In this paper, we will follow the second approach, which is more robust. Once a batch of experience has been used to do a gradient update the experience is then discarded and the policy gets improved. Due to this reason the second approach is typically more efficient because it only use the collected experience once for doing an update.

The policy on which the current agent is choosing gets optimized by directly measuring the gradient of the policy with respect to the parameters of the current policy. The objective function is defined as follows:

$$L(\theta) = \mathbb{E} [\min (X \cdot A, \text{clip} (X, 1 - \epsilon, 1 + \epsilon) \cdot A)] , \quad (2)$$

such that $X = \frac{\pi_{\theta}(a_t|s_t)}{\pi_{\theta_{old}}(a_t|s_t)}$

A is the advantage function, and θ are parameters of the policy that we want to optimize, in fact these parameters decide the probability of an action in a given state. The quantity $\frac{\pi_{\theta}(a_t|s_t)}{\pi_{\theta_{old}}(a_t|s_t)}$ is the ratio of probability of taking an action in a new policy with respect to the old policy, it signifies how much the policy has been updated. A is the advantage function which signifies how much better or worse the agent’s actions when compared with the expected return. The clip function ensures that the policy update is within a certain range: $[1 - \epsilon, 1 + \epsilon]$, where ϵ is a hyperparameter ranges from 0.1 to 0.2. Then finally either clipped or unclipped function is considered whichever is the minimum. The ‘min’ function tries to avoid any large change in the policy update.

III. A GENERAL SETUP FOR COSMOLOGICAL INFLATION

In this section, we will give a brief overview of the inflationary cosmology without resorting to any sort of cosmological model. The duration of inflation is characterized in terms of the number of e-foldings N which is generally formulated in terms of the scale factor $a(t)$, or the Hubble parameter $H(t)$ (where $t :=$ cosmic time) as [11, 19]

$$N := \int_{a_{ini}}^{a_{end}} \frac{da(t)}{a(t)} = \int_{t_{ini}}^{t_{end}} H(t) dt. \quad (3)$$

Here quantities with subscripts ‘ini’ and ‘end’ refer to the time when inflation started and ended, respectively. Typically, the duration of inflation should be ~ 60 e-folds to avoid the flatness and horizon problems. The Hubble slow-roll parameters during inflation can be expressed as

$$\epsilon_H \equiv -\frac{\dot{H}}{H^2} = -\frac{d \ln H}{dN}, \quad \text{where } \cdot \equiv \frac{d}{dt} \quad (4)$$

$$\eta_H = \epsilon_H - \frac{1}{2\epsilon_H} \frac{d\epsilon_H}{dN}, \quad (5)$$

such that the slow-roll conditions during inflation are satisfied when $\epsilon_H, \eta_H \ll 1$. If $\epsilon_H \simeq 1$, the period of inflation gets over. The observational quantities, such as the scalar spectral index n_s and tensor-to-scalar ratio r_T can be directly formulated in terms of the slow-roll parameters as

$$n_s = 1 - 4\epsilon_H + 2\eta_H, \quad (6)$$

$$r_T = 16\epsilon_H. \quad (7)$$

The constraints on n_s and r_T by Planck TT,TE,EE+lowE+lens+BK15+BAO are found to be: $n_s = 0.9668 \pm 0.0037$ and $r_T < 0.058$ at the CMB pivot scale $k_* = 0.002 \text{ Mpc}^{-1}$. The scale-dependence of the Power Spectrum of the generated curvature perturbations \mathcal{R} during inflation can be expressed as: $\mathcal{P}(k) = \mathcal{A}_s (k/k_*)^{n_s-1}$ where $\mathcal{A}_s = 2.1 \times 10^{-9}$ is the amplitude of large-scale fluctuations at the pivot scale [9, 10].

A. Large Amplitude Fluctuations

The large scale observations such as CMB provide us the information of very small phase of inflationary paradigm which corresponds to the comoving scale that exit at the beginning of the inflation. As a consequence, a major portion of the inflationary scenario is still left unprobed which may contain interesting physics. In particular, this unprobed large phase of inflation can help us to explain the origins of some of the constituents of the universe such as Dark Matter and also the production of the relic gravity waves, etc.

Despite of the fact that the large-scale universe and inhomogeneities are consistent with the Planck’s Λ CDM

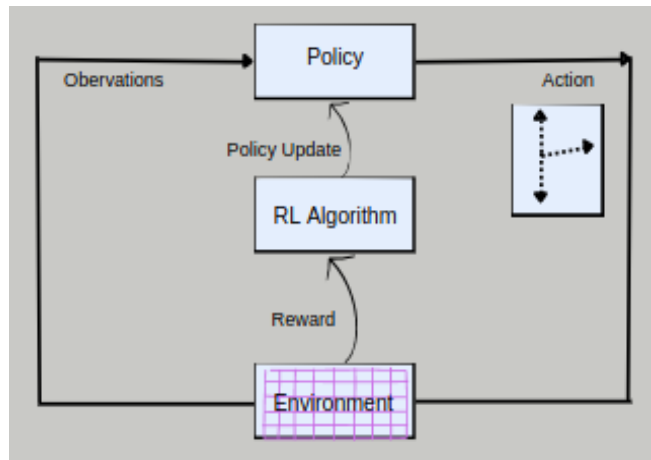


FIG. 1. This figure illustrates the Reinforcement Learning technique flowchart.

predictions, the small-scale large overdensities at some comoving wavenumber $k \gg k_* = k_{CMB}$ could arise from large density fluctuations during inflation [20–23]. Upon exiting the horizon, these fluctuations get freeze out and once they enter inside the horizon, they get collapse. If the density contrast $\delta \equiv \delta\rho/\rho \simeq 10^{-1}$, the large density perturbations, after entering inside the horizon in radiation or matter era, will get collapsed to form a PBH. The mass of primordial black holes (PBHs) can be determined from the e-foldings at which fluctuations exit the horizon. Additionally, if the distribution profile of density perturbations is known the fraction of PBHs in the total energy density of the universe can be identified.

Having the potential in explaining atleast the substantial part of DM in the form of PBH, if not all, the occurrence of large fluctuations and hence the enhanced Power spectrum upto a few orders of magnitude is actually needed [24–26]. The large amplitude of fluctuations in the inflation may generate by having ultra slow-roll (USR) inflation for a very short period of time (roughly for about a few e-folds). However, this compulsorily incorporation of a phase or phases of USR, despite being able to serve the purpose to explain the DM in the form of PBH, and the generation of Secondary Induced GWs (SIGW), requires an immense level of fine-tuning, due to which the whole scenario of generating large fluctuations seems unnatural. In order to avoid any large fine-tuning(s), at least with respect to the choosing the scale of the perturbations for large scale fluctuations, one can look for other methods or processes. In particular, those methods which evolves dynamically and search for the best-possible and more efficient way to fulfil the task.

IV. ESTABLISHMENT OF THE FRAMEWORK

In general, the inflationary framework and the one which is suited for RL to be implemented are widely dis-

connected with each other. This is due to the fact that the inflation is supposed to be governed by a scalar field which has a well-defined potential and kinetic energy, whereas, RL works well if there is a system where controlled optimization or decision-making is needed. The fact that the general setup of the inflation essentially demands the well-defined dynamics of the scalar field, aligning it with the required setup for RL poses a bigger problem. Not only this, feeding a parameterized form to the RL setup will also include the biases and cosmological assumptions associated with it, which is undesirable. So, in order to realize the inflation as well as to see the possibility of having the enhancement in the power spectrum, it becomes necessary to dynamical evolve the system in a non-parametric way. This will also ensure that the overall description of the system is not fixed beforehand and there can be many possibilities within the system.

Since, the whole dynamics of the inflation at every instant can be studied with the help of the slow-roll parameters (defined in (4)), they suit appropriate to get utilized on the basis of which the overall dynamics can be studied. Moreover, they can set to be free from any cosmological model-based assumptions. Since, the second slow-roll parameter η_H can be worked out from ϵ_H , we only need a single dynamical variable. The overall problem now can be setup in a 2-dimensional Grid-like structure which contains a wide range of discrete values of ϵ_H , approximately $\sim 10^3$. The values are generated assuming a uniform distribution given by

$$\epsilon_H \in \mathcal{U}(10^{-10}, 1). \quad (8)$$

This range also include possible values required for the enhancement of the power spectrum. The problem can now be formulated in the following way:

- We first form an environment in the form of a Grid (with dimensions $M \times N$) of ϵ_H values on which the agent will explore many times till it find the best-possible trajectory or trajectories, which is desirable according to our task ¹.
- Each cell in Grid holds a unique value of ϵ_H , known as a ‘state’. In each state, the agent takes the feedback from the environment.
- We then define a set of actions which takes the agent from one-cell to any other. Each time-step is a measure of e-foldings. Depending on which action the agent will take, the rate of change of ϵ_H will be determined at that particular time-step.

¹ Here, we note that the exploration of the agent extends beyond the neighboring states of the current grid cell. Considering the large transitions needed to achieve large η_H , we have enabled the agent to take steps of varying sizes. These steps can also alter the state value by an order of magnitude. For more details see Appendix-AVI 0e.

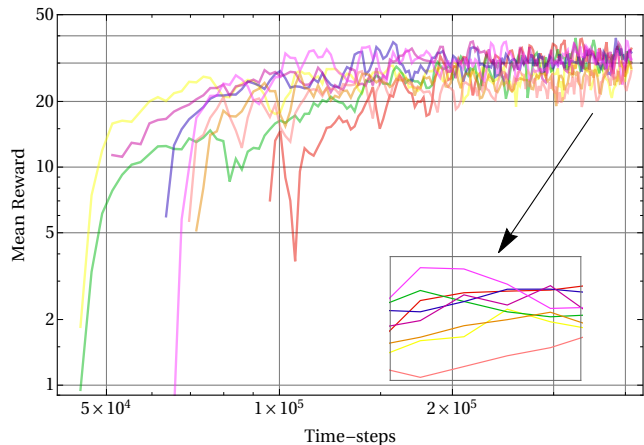


FIG. 2. This figure shows the enhancement in the mean reward throughout the training period, encompassing time-steps up to 4×10^5 . Despite originating from various initial reward values, all training sets converge towards a common mean reward as the number of time-steps progresses.

- Based on the policy updating rule (2), the agent will decide itself which action has more probability at a given time-step to enhance the reward R.
- The reward is given at each step, specifically if it satisfies the CMB constraints, slow-roll, ultra slow-roll(s), as well as at the last-step if it meets the necessary condition require to end the inflation.
- The policy gets updated after several epochs (generally ranges between 10 – 100 depending on the complexity of the system).
- The best-policy is then used to predict the outcomes, this works even if the environment gets slightly perturbed.

A. Training and Predictions

We train the build model using above-mentioned policy gradient technique of `OpenAI`. One of the reasons to choose this algorithm is its reliable performance during training in various domains and scenarios. We train our model for roughly 10^5 time steps. This procedure we have followed for a number of times to check if the seed value has any impact on the final results. Moreover, we also incorporate the randomness in the actions, which takes the agent from one cell to another, so that the system can be more further relaxed from any bias. In fig.(2) we have plotted the mean reward function with the time steps for each training process. Here one can see that even if each of the training starts with different rewards, they ultimately gets saturated to a particular value. This highlights the significance of using this algorithm as a choice and also shows that the framework is overall well-defined to make the training process smooth.

Here, we emphasize that since the environment contains rewards and penalties, the agent after getting trained learns about the environment and then behaves accordingly. The high reward at the end of the training ensures that the agent understands how to progress in such a way which gives rise to cosmological inflation in a natural and model-independent way i.e. without incorporating any cosmological model parameters, see Appendix-B (VI 0 e).

With the trained model, we checked its predictions several times, and in each prediction the agent starts with different initial value. The trained model, then gives the predictions of slow-roll parameters at each small time step, starting from the inflation to its end. Since, there is intrinsic randomness involved in the system, both in the choice of actions, as well as in the transition between the cells for a given action, the system behaves quite differently in each prediction while still satisfying all the necessary requirements. These different behaviours open the door for several possibilities which are not realized in the conventional way to generate the similar phenomenon, such as the formation of PBH and generation of SIGW. In order to check whether the predictions fulfil the demands for generating the PBH, we first need to solve the famous Mukhanov-Sasaki (MS) equation.

B. Mukhanov-Sasaki Equation

The MS equation contains the information of the evolution of the primordial density fluctuations of each mode. It characterizes the evolution of scalar metric perturbations during the inflationary epoch within a flat Friedmann-Robertson-Walker (FRW) background. The MS equation for the evolution of the comoving curvature perturbation \mathcal{R}_k or rather $v \equiv z\mathcal{R}$ ($z :=$ MS variable) for a given mode k is given by [27, 28]

$$v_k''(\tau) + \left[k^2 - \frac{z''(\tau)}{z(\tau)} \right] v_k(\tau) = 0, \quad (9)$$

where $\tau := \int dt/a(t)$ is the conformal time and ' is the derivative with respect to τ . By solving the above equation, the corresponding dimensionless Power spectrum P_k can be estimated from the following relation:

$$P_k = \frac{k^2}{2\pi^2} \left| \frac{v_k}{z} \right|^2, \quad \text{when } k \ll a(t)H(t). \quad (10)$$

For each mode k , when it is inside the sub-Hubble regime i.e. if $k \gg a(t)H(t)$, one can assume the Bunch-Davis condition in which v evolves as

$$v_k(\tau) = \frac{u_k(\tau)}{\sqrt{2k}} \exp(-ik\tau), \quad (11)$$

where $u_k(\tau)$ is a dimensionless variable. By using (9) and (11), one can write the second-order differential equation for $u_k(\tau)$ as follows: $F_k \equiv v_k^2 k + \omega_k^2 v_k^2$

$$u_k''(\tau) - (2ik)u_k'(\tau) - \frac{z''(\tau)}{z(\tau)} u_k(\tau) = 0, \quad (12)$$

where

$$\frac{z''}{z} = a^2 H^2 \left[2 - \epsilon_1 + \frac{3}{2}\epsilon_2 + \frac{1}{4}\epsilon_2^2 - \frac{1}{2}\epsilon_1\epsilon_2 + \frac{1}{2}\epsilon_2\epsilon_3 \right], \quad (13)$$

and $\epsilon_1 = \epsilon_H$, $\epsilon_{n+1} = -d \ln \epsilon_n / dN$ [29]. The above equation (12) can be numerically solved for each mode k , assuming the initial conditions $u_k(\tau)|_{ini} = 1$ and $u_k'(\tau)|_{ini} = 0$. Based on the ML predictions on the evolution of slow-roll parameters, the resulting power-spectrum profile with k can be obtained for each case.

C. Abundance of Primordial Black Holes

Let us now focus on the basic criteria for the formation of the PBH and their abundance in the universe. As we know that when universe enters in the radiation era after the end of the inflation, the fluctuations which were generated earlier and gets freeze outside the sub-Hubble region, will now enter in later times, depending on when they exited during inflation. If the size of these perturbations are very large, they produce large curvature perturbation upon re-entering the horizon which may also result in the production of the PBH [30, 31]. For each mode k , PBH of a particular mass (in terms of the solar mass M_\odot) will be generated which is given by [32]

$$\begin{aligned} M_{PBH} &:= \bar{\gamma} M_H = \bar{\gamma} \frac{4\pi}{3} \frac{\rho_{PBH}}{H^3} \\ &= 1.13 \times 10^{15} \left[\frac{g_*}{106.75} \right]^{-1/6} \left[\frac{\bar{\gamma}}{0.2} \right] \left[\frac{k_{PBH}}{k_*} \right]^{-2} M_\odot, \end{aligned} \quad (14)$$

where M_H is the Hubble mass, g_* is the total effective degree of freedom of the universe, and $\bar{\gamma}$ is known as the efficiency factor.

In order to calculate what is the total fraction of the PBHs in the universe in the form of the dark matter, we define the following quantity:

$$f_{PBH}(M_{PBH}) := \frac{\rho_{PBH}}{\rho_{DM}} = \beta(M_{PBH}) \frac{\rho_T}{\rho_{DM}}, \quad (15)$$

$$\text{where } \beta(M_{PBH}) := \frac{\rho_{PBH}}{\rho_T} \Big|_{formation}$$

and $\rho_T = 3H^2 M_{pl}^2$ is the total energy density of the universe. The Eq. (15) can also be expressed as:

$$\begin{aligned} f_{PBH}(M_{PBH}) &= 1.68 \times 10^8 \left(\frac{\bar{\gamma}}{0.2} \right)^{1/2} \left[\frac{g_*}{106.75} \right]^{-1/4} \\ &\times \left[\frac{M_{PBH}}{M_\odot} \right]^{-1/2} \beta(M_{PBH}). \end{aligned} \quad (16)$$

Here we can see from the above equation that the fraction of PBH at present epoch $t = t_0$ as a candidate for DM linearly depends on the mass fraction $\beta(M_{PBH})$. In order to calculate the latter, we resort ourselves to the Press-Schechter formalism which defines $\beta(M_{PBH})$ as the

probability that the normally distributed density perturbations are above a particular threshold value δ_c [33–35]

$$\beta(M_{PBH}) = \bar{\gamma} \int_{\delta_c}^1 \frac{d\delta}{\sqrt{2\pi}\sigma^2} \exp\left(-\frac{\delta^2}{2\sigma^2}\right), \quad (17)$$

where the standard deviation of the coarsed-grained density contrast δ is denoted by σ , which is expressed as [36]

$$\sigma^2 = \frac{16}{81} \int_0^\infty d \ln k \left(\frac{k}{k_{PBH}}\right)^4 \left[W\left(\frac{k}{k_{PBH}}\right)\right]^2 P_k \quad (18)$$

such that $W(x) := \exp\left(\frac{-x^2}{2}\right)$.

D. Induced Gravitational Waves by Scalar Perturbations

The gravitational wave (GW) spectrum is characterized by the energy density of gravitational waves (ρ_{GW}) per logarithmic unit of wavenumber, and it is normalized by the total energy density of the universe [37–39]

$$\begin{aligned} \Omega_{GW}(k, \tau) &= \frac{1}{\rho_\tau(\tau)} \frac{d\rho_{GW}}{d \ln k}, \\ &= \frac{1}{24} \left(\frac{k}{a(\tau)H(\tau)}\right)^2 \mathcal{P}_h(\tau, k), \end{aligned} \quad (19)$$

where $\mathcal{P}_h(\tau, k)$ is the dimensionless power spectrum of the tensor perturbations which in terms of the Fourier mode of the transverse-traceless part of the metric perturbations h_{ij} can be expressed as

$$\left(\frac{k^3}{2\pi^2}\right) \left[\langle h_{\mathbf{k}}^\alpha(\tau) h_{\mathbf{k}}^\beta(\tau) \rangle\right] = \delta_{\alpha\beta} \delta^3(\mathbf{k} + \bar{\mathbf{k}}) \mathcal{P}_h(\tau, k), \quad (20)$$

with α and β being the two polarization states. Following the refs. [40, 41] the induced tensor power spectrum $\mathcal{P}_h(\tau, k)$ from the second-order scalar density perturbations can be written as

$$\begin{aligned} \mathcal{P}_h(\tau, k) &= 4 \int_0^\infty da \int_{|1-a|}^{1+a} db \left(\frac{4a^2 - (1+a^2 - b^2)^2}{4ab}\right)^2 \\ &\times \mathcal{T}^2(a, b, x) P_\zeta(ka) P_\zeta(kb). \end{aligned} \quad (21)$$

Here $x = k\tau$, and $\mathcal{T}^2(a, b, x)$ is the integral kernel of secondary induced GWs [42]. To observe the $\mathcal{P}_h(\tau, k)$ at present (when $x \rightarrow \infty$) for the modes which entered during the radiation-dominated era ($w = 1/3$), the oscillating average of the integral kernel can be expressed as [43]

$$\begin{aligned} \mathcal{T}^2(a, b, \infty) &= \frac{1}{2} \left(\frac{3(a^2 + b^2 - 3)}{4(ab)^3 x}\right)^2 \\ &\times \left\{ \left[(a^2 + b^2 - 3) \log \left| \frac{3 - (a+b)^2}{3 - (a-b)^2} \right| - 4ab \right]^2 \right. \\ &\left. + \pi^2 (a^2 + b^2 - 3)^2 \theta(a + b - \sqrt{3}) \right\}, \end{aligned} \quad (22)$$

where θ is the Heaviside theta function. The spectrum of the gauge-independent GWs that is observed today $a(t) = 1$ and produced in the radiation era, is given by [44, 45]

$$\Omega_{GW}^{(0)} h^2 = \Omega_r^{(0)} h^2 \left(\frac{g_*(T_{rh})}{106.75}\right) \left(\frac{g_{*s}(T_{rh})}{106.75}\right)^{-4/3} \Omega_{GW}(k, \tau_r). \quad (23)$$

The quantities g_* and g_{*s} represent the effective degrees of freedom in the energy density and entropy evaluated at the reheating epoch, and τ_r represent the conformal time when a mode enters inside the horizon in radiation era.

V. PREDICTIVE OUTCOMES

The predictions generated by the trained RL model offer an opportunity to assess its significance in relation to the observational phenomena discussed in the previous section. In contrast to binary predictions, denoted as ‘yes’ or ‘no’, our model is specifically trained to forecast the temporal profiles of inflationary slow-roll parameters. These outcomes not only exhibit variations in their evolutionary patterns with each prediction but can also lead to entirely different scenarios or introduce features that may be absent in other predictions. Consequently, one anticipates a diverse range of evolutionary slow-roll outcomes, characterized not only by their novelty but also by their adherence to the standard inflationary constraints suggested by observational data. Moreover, this approach provides us with a statistical measure, enabling the calculation of the probability distribution function. This capability gives the method an advantage in predicting the distribution function of features of inflationary paradigm.

A. Outcomes for Scalar Power Spectrum

By obtaining predictions for the slow-roll parameters, we can systematically assess the power spectrum for each scenario. This analysis enables us to ascertain whether these scenarios conform to established cosmological patterns or exhibit distinct profiles of the spectrum. To derive the power spectrum, we numerically solve the MS equation (12) across multiple predictions. The resultant profiles are visually presented in fig. (3) for $k \in [0.002, 10^{21}] \text{ Mpc}^{-1}$. In that figure, one can discern a multitude of profiles, all satisfying the cosmic microwave background (CMB) constraint at $k = 0.002 \text{ Mpc}^{-1}$, yet demonstrating diverse evolutionary trajectories. Notably, the power spectrum manifests peaks at various k values. In numerous instances, multiple peaks (either 2 or 3) are observed, a phenomenon conventionally challenging to achieve due to the manual incorporation of features in the scalar field potential. Remarkably, in our case, this enhancement in multiple predictions occurs naturally, without necessitating any specific fine-tuning for

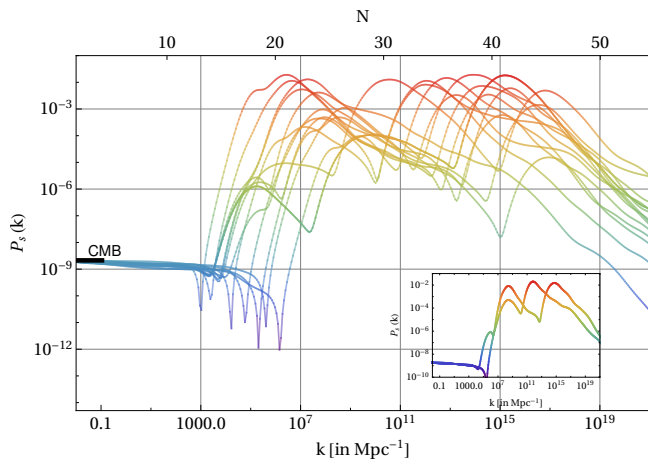


FIG. 3. This figure represents the predictive outcomes for the power spectrum in the k range $[0.002, 10^{21}] \text{ Mpc}^{-1}$. For each prediction, a particular profile is generated starting from the CMB scale. In the inset, we have plotted a couple of profiles to have a better visualization of the generated power spectrum.

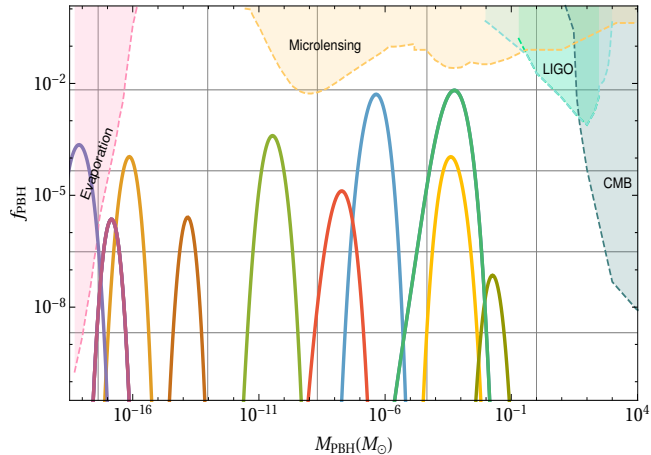


FIG. 4. This figure illustrates the proportion of dark matter in the form of PBH, denoted as f_{PBH} , for various predictions in terms of $M_{PBH}(M_{\odot})$. Each vertical contour represents a specific PBH mass with a fraction equal to or less than f_{PBH} . The shaded regions correspond to areas excluded based on various observations.

the USR period. Moreover, the extent of enhancement in the power spectrum varies across different predictions, highlighting the flexibility of our framework in providing a range of possibilities concerning peak location, amplitude, and the number of peaks.

B. Outcomes for PBH Abundance

After obtaining the power spectrum profiles for a set of generated predictions, we proceed to derive $f_{PBH}(M_{PBH})$ using Eq. (16) for each specific case. The resulting ensemble of predicted contours for f_{PBH} as a function of M_{PBH}

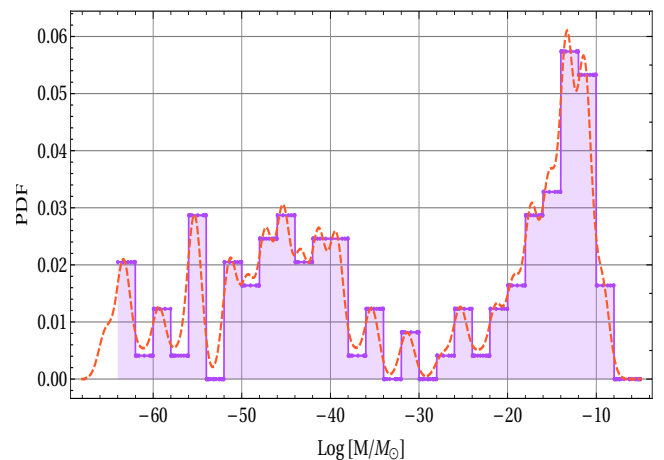


FIG. 5. This figure illustrates the probability distribution function generated from a substantial number of predictions for obtaining PBHs at a specified mass.

in the range $[10^{-18}, 10^4] M_{\odot}$ is depicted in fig. (16). In this figure, shaded areas denote excluded regions based on various observations, including CMB, GW, microlensing, and evaporation. Given that certain power spectrum profiles may lead to elevated f_{PBH} in specific PBH mass ranges, we have excluded cases that contravene observations. Additionally, it is evident from the figure that the peaks in the power spectrum generate PBHs over a range of masses rather than a specific mass. Furthermore, the abundances fall comfortably within the permissible range of observations.

In fig. (5), we have illustrated the probability distribution function (PDF) for observing a primordial black hole (PBH) with respect to the number of e-foldings (N) which corresponding to different masses. This distribution is obtained from the $f_{PBH}(M_{PBH})$ distribution shown in fig. (4). Specifically, this figure represents the probability of obtaining a PBH of a given mass. A notable observation from this figure is that the PDF tends to diminish quite early as it approaches the end of inflation. This behavior is a result of the model attempting to satisfy the necessary conditions for ending the inflation. The maximum likelihood of observing a PBH lies in the range $N \in [22, 28]$. This might be due to the fact that upto these e-folds, the model strives to sustain a sufficient amount of slow-roll period to avoid affecting the CMB constraints, and it still has a significant number of e-foldings left to smoothly end the inflation. Additionally, a secondary likelihood is observed in the power spectrum for $N \in [38, 42]$. However, beyond this range, the PDF tends to diminish as it approaches 60 e-foldings, indicating the model is trying to ensure a smooth ending to inflation. The observation of a non-vanishing PDF in the middle range values of N indicates the possibility of a significant enhancement in the power spectrum occurring at different locations. This can also be seen in fig. (3).

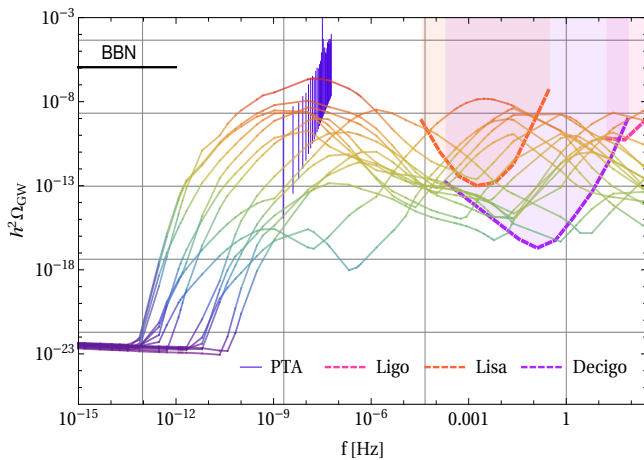


FIG. 6. This figure showcase the GW spectrum predictions as a function of frequency $f \in [10^{-15}, 500]$ Hz. The colored regions corresponds to the observational bounds from LIGO, LISA and DECIGO, and the vertical lines at frequency 10^{-9} Hz represent the observational window for the NANOGrav-15 dataset [46, 47].

C. Outcomes for SIGW

To look into the significance of the substantial enhancement observed in the scalar power spectrum, we analyze Eq. (23) to evaluate its potential detection in the present-day GW spectrum. The resulting outcomes, depicting various predictions for $\Omega_{GW}^{(0)} h^2$ across the frequency range $f \in [10^{-15}, 500]$ Hz, are illustrated in fig. (6). In this figure, the predictive spectral profiles of GW exhibit distinct behaviors from one another but consistently show enhancement in all cases. Notably, it is interesting to observe that a majority of these spectral profiles fall within the observational window of various GW observations such as LIGO, Lisa, Decigo. Notably, most of these profiles also meet the observational constraints set by NANOGrav [25, 46].

It is important to mention that the GW spectra and the current GW observations match well in two different ranges. This is particularly interesting because conventional methods typically involve highly unnatural fine-tuning of parameters to achieve such alignment. In contrast, our framework presents a well-behaved scenario that does not rely on such assumptions. It allows for the exploration of the observational implications of features in the power spectrum without the need for precise adjustment of parameters.

VI. CONCLUSION

In our pursuit to assess the utility of AI algorithm in intricate and complex scenarios, such as the generation of small-scale primordial perturbations and understanding their current cosmological observational evidence, we

introduce a novel framework in this regard. This framework brings forth intriguing possibilities that are typically obscured by the challenges posed by severe fine-tuning in such scenarios. On the build framework, we train the model using the state-of-the-art Proximal Policy Optimization algorithm and the Deep Learning architecture. The trained model is then employed to predict scalar power spectrum profiles through solving the MS equation. These profiles are subsequently utilized for studying various cosmological phenomena, including PBH abundance and the generation of SIGW.

The framework comprises a grid that encompasses all possible orders of magnitude values for the first slow-roll parameter. The agent's transitions between cells determine the second slow-roll parameter at a particular instant. Through a combination of exploration and exploitation, the agent acquires insights within the environment, determining the optimal transitions at each temporal location, starting from inflation to its end. This learning process enables the agent to fulfil necessary conditions and align with desirable ones. As the agent begins identifying the more rewarding actions at specific states, it updates its policy and explores accordingly in the subsequent episodes. After completing the training, the most recent policy is employed for predictions. However, it is essential to note that the predictions remain stochastic, aiming to achieve desirable outcomes while primarily focusing on satisfying the necessary conditions of inflation.

Once the model is trained, we apply it to generate predictions for the corresponding PBH abundance and the production of secondary-induced GWs. For the form, we utilise the standard Press-Schechter approach. We observe that, due to various peaks in the scalar power spectrum occurring at arbitrary k -locations and heights, there is a distribution of PBH abundance with mass. This is in contrast to obtaining a single-mass PBH, a common approach in the literature achieved by imposing bumps, dips, or inflection points at specific locations. Interestingly, most samples in the obtained distribution of f_{PBH} with M_{PBH} are away from the excluded regions defined by various observational limits. Notably, we not only obtain a distribution of mass but also a distribution in the maximum value of f_{PBH} for a particular mass. This highlights the intrinsic flexibility of the framework to predict outcomes without imposing fixed conditions beforehand.

Moreover, we utilize the predicted power-spectrum profiles to assess their relevance in light of the current observational constraints on the GW spectrum. Specifically, we focus on the scalar induced GW production, where the scalar power spectrum undergoes enhancement. Surprisingly, the resulting GW spectra for various predictions inherently tend to align with the constraints of small frequencies, encompassing NANOGrav, as well as those of LIGO, LISA, and DECIGO. This is noteworthy, as in many cosmological models, parameters are usually adjusted in a way that accommodates

only one set of observations at a time. Consequently, our framework not only transcends these limitations associated with model-based approaches but also identifies profiles that are unattainable in those models. In a nutshell, our approach provides a range of predictions about inflation, while trying to meet the constraints set by various observations.

ACKNOWLEDGEMENT

DFM thanks the Research Council of Norway for their support and the UNINETT Sigma2 – the National Infrastructure for High Performance Computing and Data Storage in Norway. MS is supported by Science and Engineering Research Board (SERB), DST, Government of India under the Grant Agreement number CRG/2022/004120 (Core Research Grant). MS is also partially supported by the Ministry of Education and Science of the Republic of Kazakhstan, Grant No. 0118RK00935, and CAS President’s International Fellowship Initiative (PIFI).

APPENDIX-A. DETAILS OF RL FRAMEWORK

In this appendix, we provide a comprehensive overview of our framework.

a. State-space exploration: As already mentioned, our framework comprises a rectangular grid where each cell $C_{i,j}$ contains a specific value of ϵ_H . Alongside defining states, we also need to define a set of actions:

$$A = \{a_1, a_2, a_3, \dots, a_n\}, \quad (24)$$

where each action a_i determines the extent of change the agent can induce in its state value ϵ_H . Depending on the choice of the action, the agent can make smaller steps which leads to smaller shift in the state value to mimic the slow-roll condition or it can jump over a number of cells which leads to a larger change in the state value. This is essential to mimic the bump or dip like features in the scalar field potential by enhancing the second slow-roll parameter, η_H .

b. Reward Structure: Initially, when the agent explores the environment, it can take any of actions (24) at any state, i.e. it takes any of the actions from a random uniform distribution. However, as the agent gathers information regarding which cell yields rewards or penalties, it opts to take steps that maximize its overall return of a single trajectory using an on-policy method. The agent receives rewards or penalties at each timestep based on several factors: (i) whether it satisfy n_s and r_T bound imposed by Planck 2018, (ii) whether it satisfy the slow-roll condition, (iii) whether it experiences significant changes in its state value leading to desirable enhancement in η_H , i.e. > 1 , and (iv) whether it successfully ends the inflation smoothly.

Given the infrequent occurrence of condition (iii), typically once or twice per rollout, we reward the agent more when it significantly reduces ϵ_H by several orders of magnitude. Similarly, we give larger reward for condition (iv) to meet the inflation end condition. This balances exploration across all required outcomes technically. In particular, we provide larger reward for these conditions due to their rarity as compared to the (ii) condition.

Since slow-roll conditions persist for most timesteps, therefore we give less reward. As these conditions must be met for most timesteps, the agent quickly learns actions to which satisfy slow-roll condition.

Actions resulting in conditions (iii) and (iv) receive rewards almost ten times greater than those for fulfilling the slow-roll conditions. The reason behind giving reward at each timestep is to help the agent to learn faster.

c. Model Hyperparameters: We have opted for a learning rate of 0.0003 for our training, discount factor of 0.99, clip range set at 0.2, entropy coefficient set to 0.01, batch size of 64, and ReLU activation function.

d. Exploration vs. Exploitation Strategy: During the initial stages of training, the agent encourages exploration by utilizing a stochastic policy distribution, allowing the agent to sample a variety of actions to learn about the environment. As training proceeds and the policy improves, the agent naturally reduces exploration and focuses more on exploiting the learned policy to maximize rewards. By opting for a non-zero entropy coefficient, we make sure that the agent continue to explore during training, and avoid overly deterministic policies. This choice is useful to prevent the sub-optimal convergence.

e. Diversity in predictions: As we can see in the predictions shown above such as in fig. (3), there is a noticeable diversity in the predictions, which is expected with the trained on-policy methods. The trained model effectively captures the underline probability distribution of different actions for each state within the grid which maximizes the overall return. During the prediction phase, the model selects actions based on their probabilities, which reflects some level of uncertainty in the decision-making. Therefore, the model does not strictly stick to deterministic actions at each state; instead, it leans towards choices according to their associated probabilities. It is worth noting that this behavior is not due to incomplete training but rather arises from the way the actions are being chosen based on their learned probability distributions. Consequently, both the occurrence of the USR period and the enhancement in the power spectrum contains some level of stochasticity.

APPENDIX-B. PHYSICAL INTERPRETATION OF MODEL’S PREDICTIONS

In order to see the compatibility of the obtained predictive profiles of primordial power spectrum with the

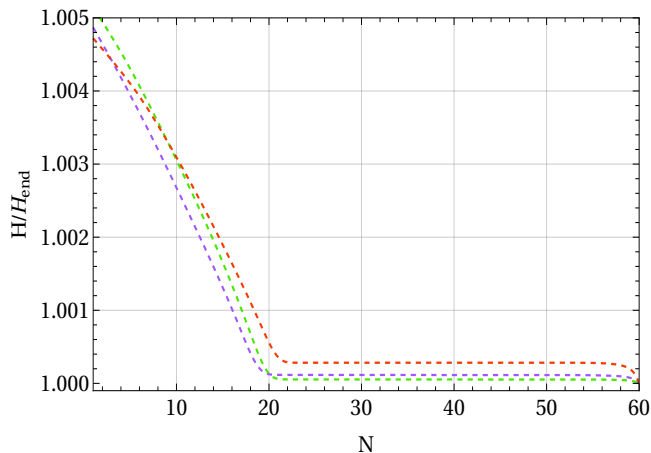


FIG. 7. Evolution of H/H_{end} with number of e-foldings $N \in [0, 60]$ for some of the model's predictions.

actual inflationary phenomena (with an ultra slow-roll period) we need to see how does the Hubble parameter is constructed out. Given the functional profiles of ϵ_H , one can directly constructed out the Hubble parameter evolution [12]

$$H(N) = H_{\text{end}} \exp \left[- \int_{60}^N \epsilon(N') dN' \right]. \quad (25)$$

In the figure (7) we demonstrated the functional profiles of $H(N)/H_{\text{end}}$ for some of the predictions on ϵ_H . Here, one can see that the Hubble parameter decreases in the beginning of the inflation and quickly approaches to H_{end} , where its variation is minuscule. This outcome is essential to realize the slow-roll regime.

To compare our results with the scalar field's inflationary scenario, we can use the standard equations:

$$H^2(t) = \frac{1}{3} \left[\frac{\dot{\phi}^2}{2} + V(\phi) \right], \quad (26)$$

$$\dot{H}(t) = -\frac{1}{2} \dot{\phi}^2. \quad (27)$$

Given that $\dot{H}(t)$ is very small from fig. (7), it is evident that the field's kinetic energy is insignificant in comparison to its potential energy. This validates the physical credibility of our results by mimicking the standard inflationary scenario.

The above fig. (7) indicates that to mimic the slow-roll or USR regime one does not need an explicitly form of with scalar field potential. Instead, one can exploit the general idea of satisfying the necessary inflationary conditions to analyze the features of the inflation.

-
- [1] Simeon Bird et al., *Did LIGO detect dark matter?*, *Phys. Rev. Lett.* **116** (2016) 201301, arXiv:1603.00464 [astro-ph.CO].
- [2] Bernard J. Carr and S. W. Hawking, *Black holes in the early Universe*, *Mon. Not. Roy. Astron. Soc.* **168** (1974) 399-415.
- [3] Bernard J. Carr, *The Primordial black hole mass spectrum*, *Astrophys. J.* **201** (1975) 1-19.
- [4] M. Sasaki, T. Suyama, T. Tanaka, S. Yokoyama, *Primordial Black Hole Scenario for the Gravitational-Wave Event GW150914*, *Phys. Rev. Lett.* **117** (2016) 061101, arXiv:1603.08338 [astro-ph.CO].
- [5] A. M. Green, B. J. Kavanagh, *Primordial Black Holes as a dark matter candidate*, *J. Phys. G* **48** (2021) 043001, arXiv:2007.10722 [astro-ph.CO].
- [6] J. Garcia-Bellido, E. Ruiz Morales, *Primordial black holes from single field models of inflation*, *Phys. Dark Univ.* **18** (2017) 47-54, arXiv:1702.03901 [astro-ph.CO].
- [7] C. Germani, T. Prokopec, *On primordial black holes from an inflection point*, *Phys. Dark Univ.* **18** (2017) 6-10, arXiv:1706.04226 [astro-ph.CO].
- [8] B. Carr, K. Kohri, Y. Sendouda, J. Yokoyama, *Constraints on primordial black holes*, *Rept. Prog. Phys.* **84** (2021) 116902, arXiv:2002.12778 [astro-ph.CO].
- [9] Planck Collaboration, Y. Akrami et al., *Planck 2018 results. X. Constraints on inflation*, *Astron. Astrophys.* **641** (2020) A10, arXiv:1807.06211 [astro-ph.CO].
- [10] N. Aghanim, et al., *Planck 2018 results. VI. Cosmological parameters*, *Astron. Astrophys.* **641** (2020) A6, arXiv:1807.06209 [astro-ph.CO].
- [11] S. S. Mishra, V. Sahni, *Primordial Black Holes from a tiny bump/dip in the Inflaton potential*, *JCAP* **04** (2020) 007, arXiv:1911.00057 [gr-qc].
- [12] O. Özsoy, G. Tasinato, *Inflation and Primordial Black Holes*, *Universe* **9** (2023) 203, arXiv:2301.03600 [astro-ph.CO].
- [13] S. Choudhury, S. Panda, M. Sami, *PBH formation in EFT of single field inflation with sharp transition*, *Phys. Lett. B* **845** (2023) 138123, arXiv:2302.05655 [astro-ph.CO].
- [14] G. Bhattacharya, S. Choudhury, K. Dey, S. Ghosh, A. Karde, *Evading no-go for PBH formation and production of SIGWs using Multiple Sharp Transitions in EFT of single field inflation*, arXiv:2309.00973 [astro-ph.CO].
- [15] M. R. Gangopadhyay, S. Myrzakul, M. Sami, M. K. Sharma, *Paradigm of warm quintessential inflation and production of relic gravity waves*, *Phys. Rev. D* **103** 043505 (2021), arXiv: 2011.09155 [astro-ph.CO].
- [16] J. Schulman, et al. *Proximal policy optimization algorithms*, arXiv:1707.06347.
- [17] Philippa S. Cole, Andrew D. Gow, Christian T. Byrnes, and Subodh P. Patil, *Primordial black holes from single-field inflation: a fine-tuning audit*, *JCAP* **08** (2023) 031, arXiv: 2304.01997 [astro-ph.CO].
- [18] S. R. Geller, W. Qin, E. McDonough, D. I. Kaiser, *Primordial black holes from multifield inflation with non-minimal couplings*, *Phys. Rev. D* **106**(6) (2022) 063535, arXiv: 2205.04471 [hep-th].
- [19] D. Baumann, *PoS TASI 2017*, 009 (2018),

- arXiv:1807.03098 [hep-th].
- [20] T. Harada, C.-M. Yoo, K. Kohri, *Threshold of primordial black hole formation*, *Phys. Rev. D* **88** (2013) 084051, arXiv:1309.4201 [astro-ph.CO].
- [21] M. R. Gangopadhyay, J. C. Jain, D. Sharma, Y. Yogesh, *Production of primordial black holes via single field inflation and observational constraints*, *Eur. Phys. J. C* **82** (2022) 849, arXiv:2108.13839 [astro-ph.CO].
- [22] R. Kimura, T. Suyama, M. Yamaguchi, Y.-L. Zhang, *Reconstruction of Primordial Power Spectrum of curvature perturbation from the merger rate of Primordial Black Hole Binaries*, *JCAP* **04** (2021) 031, arXiv:2102.05280 [astro-ph.CO].
- [23] H. Di, Y. Gong, *Primordial black holes and second order gravitational waves from ultra-slow-roll inflation*, *JCAP* **07** (2018) 007, arXiv:1707.09578 [astro-ph.CO].
- [24] S. R. Geller, W. Qin, E. McDonough, D. I. Kaiser, *Primordial black holes from multifield inflation with non-minimal couplings*, *Phys. Rev. D* **106** (2022) 063535, arXiv:2205.04471 [hep-th].
- [25] V. De Luca, G. Franciolini, A. Riotto, *NANOGrav Data Hints at Primordial Black Holes as Dark Matter*, *Phys. Rev. Lett.* **126** (2021) 041303, arXiv:2009.08268 [astro-ph.CO].
- [26] Hassan Firouzjahi, Antonio Riotto, *Sign of non-Gaussianity and the primordial black holes abundance*, *Phys. Rev. D* **108** (2023) 123504, arXiv:2309.10536 [astro-ph.CO].
- [27] H. V. Ragavendra, L. Sriramkumar, J. Silk, *Could PBHs and secondary GWs have originated from squeezed initial states?*, *JCAP* **05** (2021) 010, arXiv:2011.09938 [astro-ph.CO].
- [28] K. Inomata, E. McDonough, W. Hu, *Primordial black holes arise when the inflaton falls*, *Phys. Rev. D* **104** (2021) 123553, arXiv:2104.03972 [astro-ph.CO].
- [29] S. S. Bhatt, S. S. Mishra, S. Basak, S. N. Sahoo, *Numerical simulations of inflationary dynamics: slow-roll and beyond*, arXiv:2212.00529 [gr-qc].
- [30] G. Rigopoulos and A. Wilkins, *Inflation is always semi-classical: diffusion domination overproduces Primordial Black Holes*, *JCAP* **12** (2021) 027, arXiv:2107.05317 [astro-ph.CO].
- [31] T. Papanikolaou, *Gravitational waves induced from primordial black hole fluctuations: the effect of an extended mass function*, *JCAP* **10** (2022) 089, arXiv:2207.11041 [astro-ph.CO].
- [32] T. Nakama, J. Silk, M. Kamionkowski, *Stochastic gravitational waves associated with the formation of primordial black holes*, *Phys. Rev. D* **95** (2017) 043511, arXiv:1612.06264 [astro-ph.CO].
- [33] S. Young, C. T. Byrnes, *Primordial black holes in non-Gaussian regimes*, *JCAP* **08** (2013) 052, arXiv:1307.4995 [astro-ph.CO].
- [34] V. De Luca, A. Riotto, *A note on the abundance of primordial black holes: Use and misuse of the metric curvature perturbation*, *Phys. Lett. B* **828** (2022) 137035, arXiv:2201.09008 [astro-ph.CO].
- [35] V. De Luca, A. Kehagias, A. Riotto, *How well do we know the primordial black hole abundance: The crucial role of nonlinearities when approaching the horizon*, *Phys. Rev. D* **108** (2023) 063531, arXiv:2307.13633 [astro-ph.CO].
- [36] G. Franciolini, A. Kehagias, S. Matarrese, A. Riotto, *Primordial Black Holes from Inflation and non-Gaussianity*, *JCAP* **03** (2018) 016, arXiv:1801.09415 [astro-ph.CO].
- [37] M. Kawasaki, N. Kitajima, S. Yokoyama, *Gravitational waves from a curvaton model with blue spectrum*, *JCAP* **08** (2013) 042, arXiv:1305.4464 [astro-ph.CO].
- [38] M. A. Gorji, M. Sasaki, T. Suyama, *Extra-tensor-induced origin for the PTA signal: No primordial black hole production*, arXiv:2307.13109 [astro-ph.CO].
- [39] S. Vagnozzi, *Inflationary interpretation of the stochastic gravitational wave background signal detected by pulsar timing array experiments*, *JHEAp* **39** (2023) 81–98, arXiv:2306.16912 [astro-ph.CO].
- [40] S. Bhattacharya, S. Mohanty, P. Parashari, *Implications of the NANOGrav result on primordial gravitational waves in nonstandard cosmologies*, *Phys. Rev. D* **103** (2021) 063532, arXiv:2010.05071 [astro-ph.CO].
- [41] T. Papanikolaou, A. Lympiris, S. Lola, E. N. Saridakis, *Primordial black holes and gravitational waves from non-canonical inflation*, *JCAP* **03** (2023) 003, arXiv:2211.14900 [astro-ph.CO].
- [42] D. Baumann, P. J. Steinhardt, K. Takahashi, K. Ichiki, *Gravitational Wave Spectrum Induced by Primordial Scalar Perturbations*, *Phys. Rev. D* **76** (2007) 084019, arXiv:hep-th/0703290.
- [43] G. Franciolini, A. Junior Iovino, V. Vaskonen, H. Veermäe, *Recent Gravitational Wave Observation by Pulsar Timing Arrays and Primordial Black Holes: The Importance of Non-Gaussianities*, *Phys. Rev. Lett.* **131** (2023) 201401, arXiv:2306.17149 [astro-ph.CO].
- [44] S. Balaji, G. Domènech, G. Franciolini, *Scalar-induced gravitational wave interpretation of PTA data: the role of scalar fluctuation propagation speed*, *JCAP* **10** (2023) 041, arXiv:2307.08552 [gr-qc].
- [45] S. Maiti, D. Maity, L. Sriramkumar, *Constraining inflationary magnetogenesis and reheating via GWs in light of PTA data*, arXiv:2401.01864 [gr-qc].
- [46] NANOGrav Collaboration, G. Agazie et al., *The NANOGrav 15 yr Data Set: Evidence for a Gravitational-wave Background*, *Astrophys. J. Lett.* **951** (2023) L8, arXiv:2306.16213 [astro-ph.HE].
- [47] J. Antoniadis et al., *The second data release from the European Pulsar Timing Array - III. Search for gravitational wave signals*, *Astron. Astrophys.* **678** (2023) A50, arXiv:2306.16214 [astro-ph.HE].